Y. Wang, F. Topputo
A TFC-Based Homotopy Continuation Algorithm with Application to Dynamics and Control Problems
Journal of Computational and Applied Mathematics, In press - Published online 20/08/2021
doi:10.1016/j.cam.2021.113777

A TFC-based Homotopy Continuation Algorithm with Application to Dynamics and Control Problems

Yang Wang[a,1], Francesco Topputo [a,2,*]

[a]*Department of Aerospace Science and Technology, Politecnico di Milano, Via La Masa 34, Milan, Italy, 20156.*

Abstract

A method for solving zero-finding problems is developed by tracking homotopy paths, which define connecting channels between an auxiliary problem and the objective problem. Current algorithms' success highly relies on empirical knowledge, due to manually, inherently selected homotopy paths. This work introduces a homotopy method based on the Theory of Functional Connections (TFC). The TFC-based method implicitly defines infinite homotopy paths, from which the most promising ones are selected. A two-layer continuation algorithm is devised, where the first layer tracks the homotopy path by monotonously varying the continuation parameter, while the second layer recovers possible failures resorting to a TFC representation of the homotopy function. Compared to pseudo-arclength methods, the proposed TFC-based method retains the simplicity of direct continuation while allowing a flexible path switching. Numerical simulations illustrate the effectiveness of the presented method.

Keywords: Zero-Finding Problems, Homotopy Method, Theory of Functional Connections, Discrete Continuation, Pseudo Arclength

1. Introduction

The homotopy method is an effective technique used to tackle difficult zero-finding problems [1–5]. By traversing a series of auxiliary problems, the

*Corresponding author.
[1]PhD Candidate, yang.wang@polimi.it.
[2]Full Professor, francesco.topputo@polimi.it.

homotopy method solves the objective problem by tracking the homotopy path, which is comprised of solutions of former [6]. There are two steps for designing an effective homotopy method. The first is to construct a homotopy function, while the second is to design an algorithm to track the implicitly defined homotopy path.

For what concerns the construction of the homotopy function, many variations can be found in literature. In [7], a combination of Newton function and fixed-point function is proposed. In [8], all isolated solutions of the cyclic-n polynomial equations are found using polyhedral homotopy method. Newton homotopy method with adjustable auxiliary function is proposed in [9]. In [10], a double-homotopy method is used to construct discontinuous paths [11]. Homotopy methods from control point of view are investigated in [12, 13]. All in all, the state of the art is to define homotopy functions that yield one or few homotopy paths. As the pre-defined homotopy path is not altered during the solution process, the success of the method relies on the empirical knowledge of the objective problem.

For what concerns the tracking strategies, there are two main categories: the piecewise-linear (PL) and the predictor-corrector (PC) continuation methods [6]. PL methods follow the path by building a piecewise linear approximation of the homotopy line. The search space is subdivided into cells, and the approximation is achieved by finding the solution at faces of cells [14]. PL methods pose less requirements on the underlying equations, but they are slower and less efficient for high-dimensional problems than PC methods [6]. The latter track the path through prediction and correction stages. The simplest and most commonly used PC method is the discrete continuation method (DCM) [2]. Besides, adaptive step-size tracking was developed in [15, 16] to improve the computational efficiency of path tracking.

In DCM, the homotopy parameter varies monotonously at each step. The simplest predictor for DCM is to use the solution of the previous auxiliary problem. A variety of higher-order predictors, such as polynomial extrapolation [6] and Runge–Kutta methods [17], have been investigated. In [18], the monolithic homotopy method is formulated by integrating the predictor and corrector into a single component. An improvement of this method consists of using higher derivative information [19]. Although DCM is straightforward and easy to implement, it fails when the homotopy path encounters unfavorable conditions, such as limit points (where the Jacobian matrix is ill-conditioned) or the path goes off to infinity [10].

One enhanced PC method is the pseudo-arclength method (PAM) [6].

By reversing the homotopy path direction and augmenting the Jacobian matrix, PAM can effectively pass limit points [6]. Compared to DCM, PAM has a broader convergence domain, yet its implementation is more involved [20]. In [21, 22], the continuation parameter was extended to the complex domain to avoid singular points. However, these methods may still fail, e.g., when the homotopy path grows indefinitely [23, 24]. This in turn calls for enhancements to improve the algorithmic robustness in homotopy methods.

Apart from numerical homotopy methods, the homotopy analysis method (HAM) was developed in recent years to determine analytic approximate solutions for highly nonlinear problems [25]. Unlike perturbation techniques, the HAM is independent of any small/large physical parameters, and it provides a convenient way to guarantee the convergence of the solution series [25]. These features enable HAM to solve a wide range of difficult problems [25–27].

The Theory of Connections (ToC) has been recently proposed to investigate arbitrary connections between points [28]. The Theory of Functional Connections (TFC) extends the ToC to the functional domain [29–31]. Inspired by the conceptual similarity between homotopy and connections, a TFC-based homotopy method is presented in this paper. TFC-based homotopy implicitly defines infinite homotopy paths that connect the auxiliary problems to the objective problem. This feature paves the way to enhance the algorithm performance by leveraging the freedom in the selection of the homotopy line. A two-layer algorithm that combines DCM and TFC homotopy function is designed. Specifically, DCM is used in the first layer, while the second layer is triggered when continuation fails to advance on the current homotopy path. In the second layer, the TFC-based homotopy function is explored to search a different but feasible homotopy path. Thus, the devised method retains the easy implementation of DCM, while enabling flexible path switching. Several numerical examples are conducted to illustrate the effectiveness of the proposed method.

The paper is structured as follows. Section 2 introduces the fundamentals of homotopy methods. Section 3 outlines the TFC-based, DCM method. In Section 4, several numerical simulations are conducted. Conclusions are drawn in Section 5.

2. Fundamentals of Homotopy Methods

2.1. Homotopy Function

Consider the zero-finding problem

$$\boldsymbol{F}(\boldsymbol{x}) = \boldsymbol{0} \tag{2.1}$$

where $\boldsymbol{x} \in \mathbb{R}^n$ and $\boldsymbol{F} : \mathbb{R}^n \to \mathbb{R}^n$ is a $\mathcal{C}^2$ function. Newton's method is widely used to solve problem (2.1). However, it fails if the initial guess solution lies beyond its convergence domain, or singular points are encountered during iterations. These issues are likely in high-sensitive, nonlinear systems.

Homotopy is an effective strategy to solve difficult zero-finding problems, which lacks a priori knowledge on good initial guesses [6]. To solve (2.1), one may define a homotopy or deformation function $\boldsymbol{\Gamma}(\kappa, \boldsymbol{x}) : \mathbb{R} \times \mathbb{R}^n \to \mathbb{R}^n$ such that

$$\boldsymbol{\Gamma}(0, \boldsymbol{x}) = \boldsymbol{G}(\boldsymbol{x}), \qquad \boldsymbol{\Gamma}(1, \boldsymbol{x}) = \boldsymbol{F}(\boldsymbol{x}) \tag{2.2}$$

where $\kappa \in [0, 1]$ is the homotopy parameter and $\boldsymbol{G}(\boldsymbol{x}) : \mathbb{R}^n \to \mathbb{R}^n$ is a user-defined, auxiliary function. $\boldsymbol{G}(\boldsymbol{x})$ is usually defined to be similar to $\boldsymbol{F}(\boldsymbol{x})$, and the solution $\boldsymbol{x}_0$ to $\boldsymbol{G}(\boldsymbol{x}) = \boldsymbol{0}$ is easier to determine. The convex homotopy function is the commonly used form for $\boldsymbol{\Gamma}$:

$$\boldsymbol{\Gamma}(\kappa, \boldsymbol{x}) \coloneqq \kappa\ \boldsymbol{F}(\boldsymbol{x}) + (1 - \kappa)\ \boldsymbol{G}(\boldsymbol{x})$$

Three types of homotopy are commonly used [7], depending on $\boldsymbol{G}$:

1. Newton homotopy, $\boldsymbol{G}(\boldsymbol{x}) \coloneqq \boldsymbol{F}(\boldsymbol{x}) - \boldsymbol{F}(\boldsymbol{x}_0)$
2. Fixed-point homotopy, $\boldsymbol{G}(\boldsymbol{x}) \coloneqq \boldsymbol{x} - \boldsymbol{x}_0$
3. Affine homotopy, $\boldsymbol{G}(\boldsymbol{x}) \coloneqq A\,(\boldsymbol{x} - \boldsymbol{x}_0)$

where A is a $n \times n$ matrix.

Under regularity assumptions [6, 32], defining the homotopy function inherently generates a unique curve $\boldsymbol{c}(\theta) \coloneqq [\kappa(\theta), \boldsymbol{x}(\theta)] = \boldsymbol{\Gamma}^{-1}(\boldsymbol{0}) : J \to \mathbb{R}^{n+1}$ for some open interval $J \subset \mathbb{R}$ starting from $\boldsymbol{x}_0$, which contains points satisfying the consistency condition $\boldsymbol{\Gamma}(\kappa, \boldsymbol{x}) = \boldsymbol{0}$. θ is the continuation parameter that varies monotonously. The tracked solution curve in $\mathbb{R}^{n+1}$ is called homotopy path or zero curve. With reference to Fig. 1, the homotopy paths can be mainly classified in five Types [33]:

1) The homotopy path ends in $\{1\} \times \mathbb{R}^n$, with non-monotonic κ;
2) The homotopy path ends in $\{1\} \times \mathbb{R}^n$, with monotonic κ;

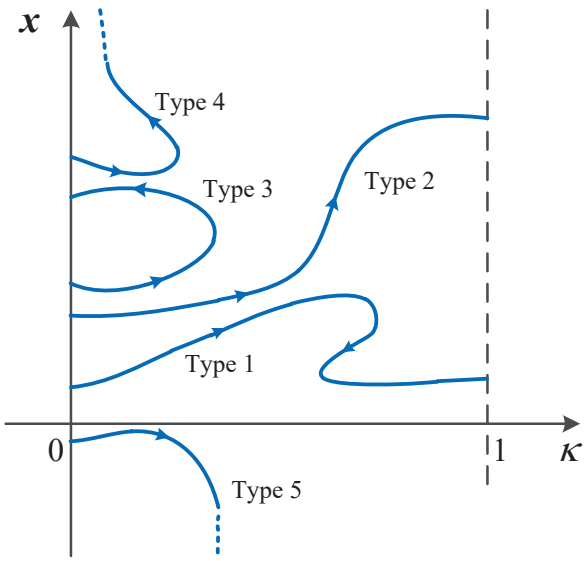

Figure 1: Different types of homotopy paths $[\boldsymbol{x}(\theta), \kappa(\theta)] = \boldsymbol{\Gamma}^{-1}(\mathbf{0})$ starting from $\kappa = 0$

.

3) The homotopy path returns to a solution of $\boldsymbol{\Gamma}(0, \boldsymbol{x})$ in $\{0\} \times \mathbb{R}^n$;
4) The homotopy path is unbounded, with non-monotonic $\kappa \in [0, 1)$;
5) The homotopy path is unbounded, with monotonic $\kappa \in [0, 1)$.

Homotopy methods attempt to track the homotopy path starting from $(0, \boldsymbol{x}_0)$ to $(1, \boldsymbol{x}^*)$. When this happens, one zero of (2.1) is found. The sufficient conditions for the existence of the homotopy path are given by probability-one homotopy theory [33, 34], based on differential geometry concepts.

Definition 2.1 (Transversality)**.** *Let $U \subset \mathbb{R}^n$ and $V \subset \mathbb{R}^p$ be open sets, and let $\boldsymbol{\rho}$: $[0, 1) \times U \times V \to \mathbb{R}^n$ be a $\mathcal{C}^2$ map. $\boldsymbol{\rho}$ is said to be transversal to zero if the Jacobian $D\boldsymbol{\rho} \in \mathbb{R}^{n \times (1+n+p)}$ has full rank on $\boldsymbol{\rho}^{-1}(\mathbf{0})$.*

Theorem 2.1 (Sard's theorem)**.** *Let $\boldsymbol{\rho}$: $[0, 1) \times U \times V \to \mathbb{R}^n$ be a $\mathcal{C}^2$ map. If $\boldsymbol{\rho}$ is transversal to zero, then for almost all $\boldsymbol{a} \in U$, the map*

$$\boldsymbol{\rho}_a(\kappa, \boldsymbol{x}) \coloneqq \boldsymbol{\rho}(\kappa, \boldsymbol{x}, \boldsymbol{a})$$

is also transversal to zero.

The parametrized Sard's theorem indicates that for almost all $\boldsymbol{a} \in U$, the zero set of $\boldsymbol{\rho}_a$ consists of smooth, nonintersecting curves [33]. In the following, we take $U \equiv \mathbb{R}^n$ and $V \equiv \mathbb{R}^p$.

Theorem 2.2 (Homotopy path)**.** *Let $\boldsymbol{\rho} : [0,1) \times \mathbb{R}^n \times \mathbb{R}^p \to \mathbb{R}^n$ be a $\mathcal{C}^2$ map, and let $\boldsymbol{\rho}_a(\kappa, \boldsymbol{x}) = \boldsymbol{\rho}(\kappa, \boldsymbol{x}, \boldsymbol{a})$. Suppose that:*

i) for each fixed $\boldsymbol{a} \in \mathbb{R}^p$, $\boldsymbol{\rho}$ is transversal to zero;
ii) $\boldsymbol{\rho}_a(0, \boldsymbol{x}) = \mathbf{0}$ has a unique nonsingular solution $\boldsymbol{x}_0$;
iii) $\boldsymbol{\rho}_a(1, \boldsymbol{x}) = \boldsymbol{F}(\boldsymbol{x})$;
iv) $\boldsymbol{\rho}_a^{-1}(\mathbf{0})$ is bounded;

then, the solution curve reaches a point $(1, \boldsymbol{x}^*)$ such that $\boldsymbol{F}(\boldsymbol{x}^*) = \mathbf{0}$. Furthermore, if $D\boldsymbol{F}(\boldsymbol{x}^*)$ is invertible, then the homotopy path has finite arc length.

Transversality is hard to verify for arbitrary $\boldsymbol{a} \in \mathbb{R}^p$, and a proper $\boldsymbol{a}$ is required to construct the homotopy function. For example, fixed-point homotopy methods require selecting a proper $\boldsymbol{x}_0$. However, in current homotopy methods [6], $\boldsymbol{a}$ is manually selected and it cannot vary during iterations. Thus, the success of the entire procedure relies heavily on the initial point chosen, and thus once again on the empirical knowledge of the problem.

Remark 2.1. *The homotopy satisfying the hypotheses of Theorem 2.2 is called a globally convergent probability-one homotopy [33]. Designing probability-one homotopy algorithms for general applications is still an open problem. Theorem 2.2 is a guideline for robust homotopy algorithm design.*

Remark 2.2. *The $\mathcal{C}^2$ class is required for $\boldsymbol{\rho}$, and this condition cannot be relaxed [33]. $\mathcal{C}^2$ is used to ease the following arguments.*

Remark 2.3. *Predicting the homotopy path in the later iterations is generally difficult, unless the conditions of Theorem 2.2 are satisfied or the problem is simple enough (see the example in [24]). The behavior in the small neighborhood of current solution point is known if the conditions of Implicit Function Theorem are satisfied.*

2.2. Path Tracking Methods

Once the homotopy function is defined, the focus is on tracking its implicitly defined path. Two predictor-corrector methods are reviewed: discrete continuation method (DCM) and pseudo-arclength method (PAM).

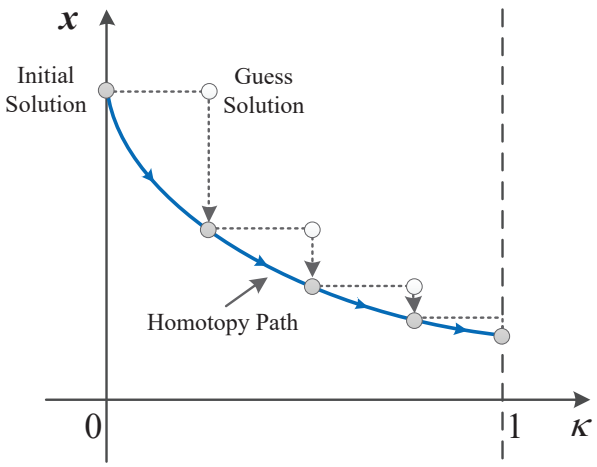

Figure 2: Graphical interpretation of DCM.

2.2.1. Discrete Continuation Method

DCM tries to solve $\mathbf{\Gamma}(\kappa, \boldsymbol{x}) = \mathbf{0}$ with monotonous variation of κ [14], i.e., $\theta \coloneqq \kappa$. The solution curve $\boldsymbol{c}(\theta)$ is reduced as $\boldsymbol{c}(\theta) \coloneqq \boldsymbol{x}(\kappa)$ As shown in Fig. 2, starting from initial solution at $\kappa = 0$, DCM solves the next solution on homotopy path using the former solution as initial guess. This process continues until the $\kappa = 1$ line is reached. DCM is simple and easy to implement, but it fails when the homotopy path exhibits limit points (Type 1, 3, 4) or goes off to infinity (Type 5). Limit points are points where the Jacobian $\mathbf{\Gamma}_{\boldsymbol{x}}(\kappa, \boldsymbol{x})$ is singular, thus DCM cannot continue by monotonously varying κ [10]. In Fig. 2, the simple zero-order DCM method is shown. In principles, one can construct a higher-order predictor using polynomial extrapolation [6]. This could result in a more efficient algorithm, yet higher-order DCM will still fail at limit points. Another type of singular points are bifurcation points where homotopy path branches emanate [10]. For the problems considered in this work, it is assumed that DCM failure is caused by limit points or infinite paths.

2.2.2. Pseudo-Arclength Method

PAM is an alternative to pass limit points that uses the arclength s as the continuation variable θ. Suppose that a solution point $(\kappa_i, \boldsymbol{x}_i)$ satisfies the consistency condition and its unit tangent direction $(\hat{\kappa}_i, \hat{\boldsymbol{x}}_i)$ is known, where the hat is the derivative w.r.t. s. In order to find the next solution point

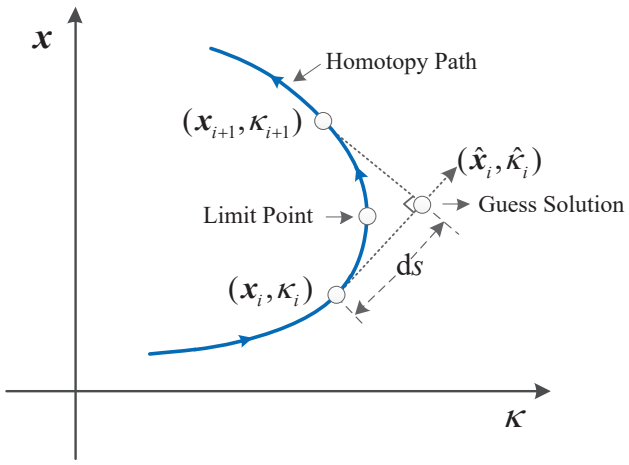

Figure 3: Graphical interpretation of PAM near a limit point.

$(\kappa_{i+1}, \boldsymbol{x}_{i+1})$, the following augmented system is to be solved for $(\kappa, \boldsymbol{x})$

$$\begin{cases} \boldsymbol{\Gamma}(\kappa, \boldsymbol{x}) = \boldsymbol{0} \\ (\boldsymbol{x} - \boldsymbol{x}_i)^\top \hat{\boldsymbol{x}}_i + (\kappa - \kappa_i)\, \hat{\kappa}_i - \mathrm{d}s = 0 \end{cases} \tag{2.3}$$

The augmented Jacobian of system (2.3) evaluated at $(\kappa_i, \boldsymbol{x}_i)$, that is,

$$\boldsymbol{J}_a(\kappa_i, \boldsymbol{x}_i) = \begin{bmatrix} \boldsymbol{\Gamma}_x(\kappa_i, \boldsymbol{x}_i) & \boldsymbol{\Gamma}_\kappa(\kappa_i, \boldsymbol{x}_i) \\ \hat{\boldsymbol{x}}_i^\top & \hat{\kappa}_i \end{bmatrix}$$

is generally regular [6].

The ability of PAM to pass a limit point is graphically shown in Fig. 3. When a limit point is approached, PAM attempts to track the homotopy path by predicting the solution along the tangent direction, and refining the solution until system (2.3) is solved. Geometrically, the solution curve continues on the opposite κ direction (in Fig. 3, κ decreases across the limit point). PAM can elegantly satisfy condition i) in Theorem 2.2, but it still fails when dealing with homotopy path Types 3–5. Compared to DCM, PAM has broader convergence domain, but its implementation is more involved [20].

3. Theory of Functional Connection Homotopy Method

3.1. Theory of Functional Connections

The Theory of Functional Connections (TFC) is the extension of the Theory of Connections (TOC) [28]. The latter investigates the arbitrary

connections between points by constructing a constrained function expressed in terms of an auxiliary function [28]. It has the property that no matter what the auxiliary function is, the constrained function always satisfies a prescribed set of constraints.

Suppose we define the scalar function

$$y(\eta) \coloneqq g(\eta) + \frac{\eta - \eta_0}{\eta_f - \eta_0}(y_f - g_f) + \frac{\eta_f - \eta}{\eta_f - \eta_0}(y_0 - g_0) \tag{3.1}$$

where $y(\eta)$ and $g(\eta)$ are the *constrained function* and *auxiliary function*, respectively, whereas $\eta \in [\eta_0, \eta_f]$ is the independent variable. It is easy to verify that (3.1) inherently satisfies $y(\eta_0) = y_0$ and $y(\eta_f) = y_f$ regardless of the specific choice of $g(\eta)$ (note that $g_0 = g(\eta_0)$ and $g_f = g(\eta_f)$). Therefore, the line $y(\eta)$ will always connect the points $P_0 = (\eta_0, y_0)$ and $P_f = (\eta_f, y_f)$. Equation (3.1) is the generalization of interpolation formulae: it is not the interpolating expression for a class of functions but for all functions [28].

In the multi-dimensional case, the two-point condition is

$$\boldsymbol{y}(\eta_0) = \boldsymbol{y}_0, \qquad \boldsymbol{y}(\eta_f) = \boldsymbol{y}_f \tag{3.2}$$

where $\boldsymbol{y} \in \mathbb{R}^n$. The general expression of the constrained function $\boldsymbol{y}(\eta)$ is

$$\boldsymbol{y}(\eta) = \boldsymbol{g}(\eta) + P_1(\eta)\boldsymbol{c}_1 + P_2(\eta)\boldsymbol{c}_2 \tag{3.3}$$

where $P_{1,2} : \mathbb{R} \to \mathbb{R}^{n\times n}$ are matrices whose elements are scalar-valued functions of η, while $\boldsymbol{c}_{1,2} \in \mathbb{R}^n$ are constant vectors of weights [28]. Substituting (3.2) into (3.3) and solving for $\boldsymbol{c}_{1,2}$ yields

$$\begin{bmatrix}\boldsymbol{c}_1\\ \boldsymbol{c}_2\end{bmatrix} = \begin{bmatrix}P_1(\eta_0) & P_2(\eta_0)\\ P_1(\eta_f) & P_2(\eta_f)\end{bmatrix}^{-1}\begin{bmatrix}\boldsymbol{y}_0 - \boldsymbol{g}_0\\ \boldsymbol{y}_f - \boldsymbol{g}_f\end{bmatrix} = \begin{bmatrix}Q_{11} & Q_{12}\\ Q_{21} & Q_{22}\end{bmatrix}\begin{bmatrix}\boldsymbol{y}_0 - \boldsymbol{g}_0\\ \boldsymbol{y}_f - \boldsymbol{g}_f\end{bmatrix} \tag{3.4}$$

where again $\boldsymbol{g}_0 = \boldsymbol{g}(\eta_0)$ and $\boldsymbol{g}_f = \boldsymbol{g}(\eta_f)$. Moreover

$$\begin{aligned} Q_{11} &= \left[P_1(\eta_0) - P_2(\eta_0)P_2^{-1}(\eta_f)P_1(\eta_f)\right]^{-1}\\ Q_{21} &= -P_2^{-1}(\eta_f)P_1(\eta_f)\ Q_{11}\\ Q_{12} &= -P_1^{-1}(\eta_0)P_2(\eta_0)\ Q_{22}\\ Q_{22} &= \left[P_2(\eta_f) - P_1(\eta_f)P_1^{-1}(\eta_0)P_2(\eta_0)\right]^{-1}\end{aligned} \tag{3.5}$$

The selection of $P_{1,2}(\eta)$ in (3.3) must ensure the existence of Q_{ij} in (3.5). Substituting (3.4) into (3.3) gives the general form of constrained function

$$\boldsymbol{y}(\eta) = \boldsymbol{g}(\eta) + \sum_{i=1}^{2} P_i(\eta)Q_{i1}(\boldsymbol{y}_0 - \boldsymbol{g}_0) + \sum_{i=1}^{2} P_i(\eta)Q_{i2}(\boldsymbol{y}_f - \boldsymbol{g}_f) \tag{3.6}$$

The constrained function $\boldsymbol{y}(\eta)$ in (3.6) defines arbitrary connection paths between $\boldsymbol{y}_0$ and $\boldsymbol{y}_f$ produced by the infinitely possible choices of $\boldsymbol{g}(\eta)$. The constrained function for arbitrary boundary conditions can also be established [28]. The Theory of Functional Connections (TFC) extends the idea above to construct the constrained function on a functional domain [29].

3.2. TFC-Based Homotopy Function

From a geometrical point of view, the homotopy function defines the solution curve connecting the two zero-finding problems defined at the boundaries of κ, which satisfy (2.2). Analogously, the constrained function in the TFC connects points at the boundaries of η. Interpreting the constrained function as describing an homotopy path is therefore natural.

In (3.6), replacing the constrained function $\boldsymbol{y}(\eta)$ by the homotopy function $\boldsymbol{\Gamma}(\eta, \boldsymbol{x})$, and $\boldsymbol{y}_0$, $\boldsymbol{y}_f$ by $\boldsymbol{G}(\boldsymbol{x})$, $\boldsymbol{F}(\boldsymbol{x})$, respectively, we have

$$\boldsymbol{\Gamma}(\eta, \boldsymbol{x}) = \boldsymbol{g}(\eta) + \sum_{i=1}^{2} P_i(\eta) Q_{i1}(\boldsymbol{G}(\boldsymbol{x}) - \boldsymbol{g}_0) + \sum_{i=1}^{2} P_i(\eta) Q_{i2}(\boldsymbol{F}(\boldsymbol{x}) - \boldsymbol{g}_f) \quad (3.7)$$

The auxiliary function $\boldsymbol{g}(\eta)$ can be expressed as a linear combination of basis functions with corresponding weights, that is

$$\boldsymbol{g}(\eta) = \Omega \boldsymbol{h}(\eta) \quad (3.8)$$

where $\boldsymbol{h}(\eta) : \mathbb{R} \to \mathbb{R}^m$ is the vector of basis functions, whereas $\Omega \in \mathbb{R}^{n \times m}$ is the matrix of weights. Note that $\boldsymbol{g}_0 = \Omega \boldsymbol{h}_0$ and $\boldsymbol{g}_f = \Omega \boldsymbol{h}_f$, where $\boldsymbol{h}_0 = \boldsymbol{h}(\eta_0)$ and $\boldsymbol{h}_f = \boldsymbol{h}(\eta_f)$. A linear map between $\kappa \in [0, 1]$ and $\eta \in [\eta_0, \eta_f]$ is also used:

$$\eta(\kappa) = (1 - \kappa)\, \eta_0 + \kappa\, \eta_f \quad (3.9)$$

Substituting (3.8) and (3.9) into (3.7) yields

$$\boldsymbol{\Gamma}(\kappa, \boldsymbol{x}, \Omega) = \Omega \boldsymbol{h}(\kappa) + \sum_{i=1}^{2} P_i(\kappa) Q_{i1} \left(\boldsymbol{G}(\boldsymbol{x}) - \Omega \boldsymbol{h}_0\right) + \sum_{i=1}^{2} P_i(\kappa) Q_{i2} \left(\boldsymbol{F}(\boldsymbol{x}) - \Omega \boldsymbol{h}_f\right) \quad (3.10)$$

Notice that $\boldsymbol{\Gamma}$ in (3.10), beside the natural dependence on κ and $\boldsymbol{x}$, is also a function of the free parameter Ω, which can be varied to steer the solution curve from $\boldsymbol{G}^{-1}(\boldsymbol{0})$ to $\boldsymbol{F}^{-1}(\boldsymbol{0})$.

It is convenient to isolate in (3.10) the part depending on κ and $\boldsymbol{x}$ only

$$\boldsymbol{\Gamma}(\kappa, \boldsymbol{x}, \Omega) = \Omega \left(\boldsymbol{h}(\kappa) - \sum_{i=1}^{2} P_i(\kappa) Q_{i1} \boldsymbol{h}_0 - \sum_{i=1}^{2} P_i(\kappa) Q_{i2} \boldsymbol{h}_f \right) + \boldsymbol{\Gamma}_0(\kappa, \boldsymbol{x}) \tag{3.11}$$

where

$$\boldsymbol{\Gamma}_0(\kappa, \boldsymbol{x}) \coloneqq \sum_{i=1}^{2} P_i(\kappa) Q_{i1} \boldsymbol{G}(\boldsymbol{x}) + \sum_{i=1}^{2} P_i(\kappa) Q_{i2} \boldsymbol{F}(\boldsymbol{x})$$

By taking the partial derivative of (3.11) w.r.t. $\boldsymbol{x}$, we find that

$$\frac{\partial \boldsymbol{\Gamma}(\kappa, \boldsymbol{x}, \Omega)}{\partial \boldsymbol{x}} = \frac{\partial \boldsymbol{\Gamma}_0(\kappa, \boldsymbol{x})}{\partial \boldsymbol{x}}$$

indicating that when a limit point is encountered, both Jacobian matrices are singular, regardless of the selection of Ω. In order to regularize $\partial \boldsymbol{\Gamma} / \partial \boldsymbol{x}$ by varying Ω, we let the basis functions $\boldsymbol{h}$ to depend on the present solution $\boldsymbol{x}$ as well; that is, $\boldsymbol{h} = \boldsymbol{h}(\kappa, \boldsymbol{x})$. Thus, (3.11) becomes

$$\boldsymbol{\Gamma}(\kappa, \boldsymbol{x}, \Omega) = \Omega \boldsymbol{\Gamma}_\Omega(\kappa, \boldsymbol{x}) + \boldsymbol{\Gamma}_0(\kappa, \boldsymbol{x}) \tag{3.12}$$

where

$$\boldsymbol{\Gamma}_\Omega(\kappa, \boldsymbol{x}) \coloneqq \boldsymbol{h}(\kappa, \boldsymbol{x}) - \sum_{i=1}^{2} P_i(\kappa) Q_{i1} \boldsymbol{h}_0(\boldsymbol{x}) - \sum_{i=1}^{2} P_i(\kappa) Q_{i2} \boldsymbol{h}_f(\boldsymbol{x})$$

Inspired by (3.12), the formal definition of TFC-based homotopy is given.

Definition 3.1 (TFC-based homotopy function)**.** *Let $\hat{\boldsymbol{\rho}}(\kappa, \boldsymbol{x}, \boldsymbol{\varepsilon}, \boldsymbol{a}) : [0, 1) \times \mathbb{R}^n \times \mathbb{R}^q \times \mathbb{R}^p \to \mathbb{R}^n$ be a $\mathcal{C}^2$ map, and let $\hat{\boldsymbol{\rho}}_a(\kappa, \boldsymbol{x}, \boldsymbol{\varepsilon}) = \hat{\boldsymbol{\rho}}(\kappa, \boldsymbol{x}, \boldsymbol{\varepsilon}, \boldsymbol{a})$ for fixed $\boldsymbol{a}$. $\hat{\boldsymbol{\rho}}_a(\kappa, \boldsymbol{x}, \boldsymbol{\varepsilon})$ is called TFC-based homotopy function if*

i) it automatically satisfies the boundary conditions

$$\hat{\boldsymbol{\rho}}_a(0, \boldsymbol{x}, \boldsymbol{\varepsilon}) = \boldsymbol{G}(\boldsymbol{x}) \qquad \text{and} \qquad \hat{\boldsymbol{\rho}}_a(1, \boldsymbol{x}, \boldsymbol{\varepsilon}) = \boldsymbol{F}(\boldsymbol{x})$$

for arbitrary $\boldsymbol{\varepsilon}$;

ii) $\forall \kappa \in (0, 1)$ and $\forall \boldsymbol{x} \in \mathbb{R}^n$, $\exists\ \boldsymbol{\varepsilon}$ such that $\partial \hat{\boldsymbol{\rho}}_a(\kappa, \boldsymbol{x}, \boldsymbol{\varepsilon}) / \partial \boldsymbol{x}$ is regular.

In traditional homotopy methods (e.g., Newton homotopy), the term $\boldsymbol{a}$ in the homotopy function $\boldsymbol{\rho}_a(\kappa, \boldsymbol{x})$ in Theorem 2.1 is set at the beginning of the continuation procedure (e.g., by providing the solution $\boldsymbol{x}_0$ to the initial problem $\boldsymbol{G}(\boldsymbol{x}) = \boldsymbol{0}$) and so is the homotopy path. The TFC-based homotopy function $\hat{\boldsymbol{\rho}}_a(\kappa, \boldsymbol{x}, \boldsymbol{\varepsilon})$ is the generalization of $\boldsymbol{\rho}_a(\kappa, \boldsymbol{x})$. Here, although $\boldsymbol{a}$ is fixed, $\boldsymbol{\varepsilon}$ brings in flexibility in the homotopy path while not affecting the boundary conditions (2.2). The TFC-based homotopy function implicitly defines infinite homotopy paths because of the infinite possible selections of $\boldsymbol{\varepsilon}$. Moreover, condition ii) in Definition 3.1 enables regularizing the path by varying $\boldsymbol{\varepsilon}$. Therefore, it is a tool to recover improperly defined paths, by detecting them and switching to different, yet feasible, homotopy paths.

Equation (3.12) provides a general form of TFC-based homotopy function. Here, $\boldsymbol{\Gamma}_0(\kappa, \boldsymbol{x})$ is equivalent to $\boldsymbol{\rho}_a(\kappa, \boldsymbol{x})$ and Ω can be seen as $\boldsymbol{\varepsilon}$ (see Remark 3.1). Let $\tau = e^{\eta_0 - \eta_f}$, the following three examples are given based on different choice of $P_{1,2}(\eta)$

1. For $P_1 = I$ and $P_2 = \eta I$

$$\boldsymbol{\Gamma}(\kappa, \boldsymbol{x}, \Omega) = \Omega\left(\boldsymbol{h}(\kappa, \boldsymbol{x}) + (\kappa - 1)\boldsymbol{h}_0(\boldsymbol{x}) - \kappa \boldsymbol{h}_f(\boldsymbol{x})\right) + \boldsymbol{\Gamma}_0(\kappa, \boldsymbol{x}) \quad (3.13)$$

2. For $P_1 = I$ and $P_2 = e^{\eta} I$

$$\boldsymbol{\Gamma}(\kappa, \boldsymbol{x}, \Omega) = \Omega\left(\boldsymbol{h}(\kappa, \boldsymbol{x}) - \frac{1 - \tau^{(1-\kappa)}}{1 - \tau}\boldsymbol{h}_0(\boldsymbol{x}) - \frac{-\tau + \tau^{(1-\kappa)}}{1 - \tau}\boldsymbol{h}_f(\boldsymbol{x})\right) + \boldsymbol{\Gamma}_0(\kappa, \boldsymbol{x}) \quad (3.14)$$

3. For $P_1 = I$ and $P_2 = e^{-\eta} I$

$$\boldsymbol{\Gamma}(\kappa, \boldsymbol{x}, \Omega) = \Omega\left(\boldsymbol{h}(\kappa, \boldsymbol{x}) - \frac{\tau - \tau^{\kappa}}{\tau - 1}\boldsymbol{h}_0(\boldsymbol{x}) - \frac{-1 + \tau^{\kappa}}{\tau - 1}\boldsymbol{h}_f(\boldsymbol{x})\right) + \boldsymbol{\Gamma}_0(\kappa, \boldsymbol{x}) \quad (3.15)$$

Remark 3.1. *Let $\Omega_{\text{col}} = \text{vec}(\Omega) \in \mathbb{R}^{\text{mn}\times 1}$, where 'vec' is an operator that converts matrices into column vectors. Then, $\Omega\boldsymbol{\Gamma}_\Omega(\kappa, \boldsymbol{x}) = \tilde{\boldsymbol{\Gamma}}_\Omega(\kappa, \boldsymbol{x})\Omega_{\text{col}}$, where*

$$\tilde{\boldsymbol{\Gamma}}_\Omega(\kappa, \boldsymbol{x}) \coloneqq \begin{bmatrix} \tilde{\boldsymbol{h}}^\top(\kappa, \boldsymbol{x}) & & & \\ & \tilde{\boldsymbol{h}}^\top(\kappa, \boldsymbol{x}) & & \\ & & \ddots & \\ & & & \tilde{\boldsymbol{h}}^\top(\kappa, \boldsymbol{x}) \end{bmatrix} \in \mathbb{R}^{n \times mn}$$

and

$$\tilde{\boldsymbol{h}}(\kappa, \boldsymbol{x}) \coloneqq \left(\boldsymbol{h}(\kappa, \boldsymbol{x}) - \sum_{i=1}^{2} P_i(\kappa) Q_{i1} \boldsymbol{h}_0(\boldsymbol{x}) - \sum_{i=1}^{2} P_i(\kappa) Q_{i2} \boldsymbol{h}_f(\boldsymbol{x}) \right)$$

Thus, Ω can be seen as a column vector $\boldsymbol{\varepsilon} \in \mathbb{R}^q$ where $q = mn$.

3.3. Regularization

This section shows the sufficient conditions for point ii) in Definition 3.1.

Lemma 3.1. *Suppose that a matrix $A \in \mathbb{R}^{n \times n}$ is the product of two matrices $B \in \mathbb{R}^{n \times m}$ and $C \in \mathbb{R}^{m \times n}$; $A = BC$. If $m < n$, then A is singular.*

Proof. Consider the linear equation

$$C\boldsymbol{x} = \boldsymbol{0}$$

if $m < n$, the number of equations is less than that of unknowns, thus there exists nonzero solution $\tilde{\boldsymbol{x}}$ such that

$$C\tilde{\boldsymbol{x}} = \boldsymbol{0}$$

then

$$BC\tilde{\boldsymbol{x}} = A\tilde{\boldsymbol{x}} = \boldsymbol{0}$$

indicating that the matrix A is singular. □

Lemma 3.2. *If $A \in \mathbb{R}^{m \times n}$ is full row rank and $m \leq n$, then $B = AA^\top \in \mathbb{R}^{m \times m}$ is regular.*

Proof. Consider the linear equation

$$B\boldsymbol{x} = AA^\top \boldsymbol{x} = \boldsymbol{0}$$

which equals to

$$\boldsymbol{x}^\top AA^\top \boldsymbol{x} = \left(A^\top \boldsymbol{x}\right)^\top A^\top \boldsymbol{x} = \boldsymbol{0} \;\rightarrow\; A^\top \boldsymbol{x} = \boldsymbol{0}$$

Since $m \leq n$ and A is full row rank, thus $\boldsymbol{x} = \boldsymbol{0}$. Therefore, B is regular. □

Theorem 3.1 (Sufficient Conditions)**.** *Let $\boldsymbol{\Gamma}(\kappa, \boldsymbol{x}, \Omega) = \Omega \boldsymbol{\Gamma}_\Omega(\kappa, \boldsymbol{x}) + \boldsymbol{\Gamma}_0(\kappa, \boldsymbol{x})$ be a candidate TFC-based homotopy function. If $m = n$ and $\partial \boldsymbol{\Gamma}_\Omega(\kappa, \boldsymbol{x})/\partial \boldsymbol{x} \in \mathbb{R}^{m \times n}$ is regular, then $\exists\ \Omega \in \mathbb{R}^{n \times m}$ such that $\partial \boldsymbol{\Gamma}(\kappa, \boldsymbol{x}, \Omega)/\partial \boldsymbol{x}$ is regular.*

Proof. Taking the derivative of (3.12) w.r.t. $\boldsymbol{x}$ yields

$$\frac{\partial \boldsymbol{\Gamma}(\kappa, \boldsymbol{x}, \Omega)}{\partial \boldsymbol{x}} = \Omega \frac{\partial \boldsymbol{\Gamma}_\Omega(\kappa, \boldsymbol{x})}{\partial \boldsymbol{x}} + \frac{\partial \boldsymbol{\Gamma}_0(\kappa, \boldsymbol{x})}{\partial \boldsymbol{x}}$$

Applying singular value decomposition to $\partial \boldsymbol{\Gamma}_0(\kappa, \boldsymbol{x})/\partial \boldsymbol{x}$, there exists

$$\frac{\partial \boldsymbol{\Gamma}_0(\kappa, \boldsymbol{x})}{\partial \boldsymbol{x}} = U^\top \begin{bmatrix} \Sigma_1 & \\ & \Sigma_2 \end{bmatrix} V$$

where Σ_1 are nonzero singular values, and Σ_2 are zero singular values if $\partial \boldsymbol{\Gamma}_0(\kappa, \boldsymbol{x})/\partial \boldsymbol{x}$ is singular. U and V are corresponding singular vectors. We can construct a regular matrix $S \in \mathbb{R}^{n \times n}$ as

$$S = U^\top \begin{bmatrix} \Lambda_1 & \\ & \Lambda_2 \end{bmatrix} V$$

where Λ_1 and Λ_2 are non-zero singular values. There always exists Λ_1 and Λ_2 such that the matrix

$$\frac{\partial \boldsymbol{\Gamma}(\kappa, \boldsymbol{x}, \Omega)}{\partial \boldsymbol{x}} = S + \frac{\partial \boldsymbol{\Gamma}_0(\kappa, \boldsymbol{x})}{\partial \boldsymbol{x}} = U^\top \begin{bmatrix} \Lambda_1 + \Sigma_1 & \\ & \Lambda_2 + \Sigma_2 \end{bmatrix} V \in \mathbb{R}^{n \times n}$$

is regular. Let $S \coloneqq \Omega \, \partial \boldsymbol{\Gamma}_\Omega(\kappa, \boldsymbol{x})/\partial \boldsymbol{x}$. From Lemma 3.1, this requires $m \geq n$. Since $\partial \boldsymbol{\Gamma}_\Omega(\kappa, \boldsymbol{x})/\partial \boldsymbol{x}$ is full rank and $m = n$, from Lemma 3.2, $\exists\ \Omega$ such that

$$\Omega = S \left(\frac{\partial \boldsymbol{\Gamma}_\Omega(\kappa, \boldsymbol{x})}{\partial \boldsymbol{x}} \right)^\top \left[\left(\frac{\partial \boldsymbol{\Gamma}_\Omega(\kappa, \boldsymbol{x})}{\partial \boldsymbol{x}} \right) \left(\frac{\partial \boldsymbol{\Gamma}_\Omega(\kappa, \boldsymbol{x})}{\partial \boldsymbol{x}} \right)^\top \right]^{-1}$$

□

According to Theorem 3.1, the following criteria are provided. Firstly, $m = n$. Secondly, monotonous functions such as exponential functions are preferred to construct each element of $\boldsymbol{h}(\kappa, \boldsymbol{x})$. Thirdly, the selection of $\boldsymbol{h}(\kappa, \boldsymbol{x})$ should consider the concrete form of TFC homotopy function. In (3.13)–(3.15), $\boldsymbol{h}(\kappa, \boldsymbol{x})$ should be nonlinear in κ to ensure the explicit dependence of $\boldsymbol{\Gamma}_\Omega(\kappa, \boldsymbol{x})$ on κ. In Section 4, the TFC homotopy function in (3.13) is used. The state-dependent basis function $\boldsymbol{h}(\kappa, \boldsymbol{x})$ is constructed as

$$\boldsymbol{h}(\kappa, \boldsymbol{x}) = \begin{bmatrix} \mathrm{e}^{x_1} \kappa^2 \\ \mathrm{e}^{x_2} \kappa^2 \\ \vdots \\ \mathrm{e}^{x_n} \kappa^2 \end{bmatrix}$$

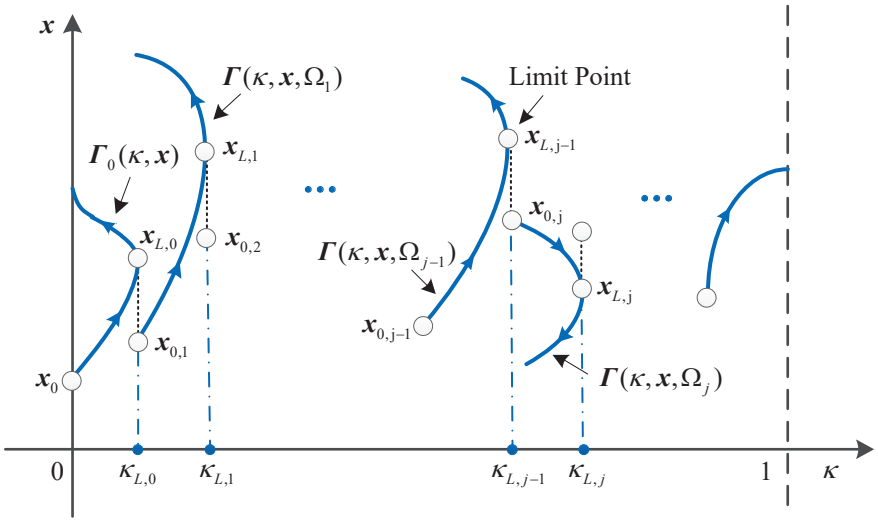

Figure 4: Graphical layout of the singular point management.

and then $\mathbf{\Gamma}_\Omega$ becomes

$$\mathbf{\Gamma}_\Omega(\kappa, \boldsymbol{x}) = \begin{bmatrix} \mathrm{e}^{x_1}(\kappa^2 - \kappa) \\ \mathrm{e}^{x_2}(\kappa^2 - \kappa) \\ \vdots \\ \mathrm{e}^{x_n}(\kappa^2 - \kappa) \end{bmatrix}$$

Thus, since the derivative of $\mathrm{e}^{x_i}, i = 1, 2, \cdots, n$, is not zero, the Jacobian of $\mathbf{\Gamma}_\Omega$ w.r.t. $\boldsymbol{x}$ is regular, $\forall \kappa \in (0, 1)$.

3.4. A Two-Layer TFC-based DCM Algorithm

Following the definition of the TFC-based homotopy function in (3.12), a two-layer DCM algorithm is proposed.

3.4.1. Singular Point Management

Fig. 4 illustrates the method, with a focus on limit point management. Starting from $\boldsymbol{x}_0$ at $\kappa = 0$, the DCM is used first to track the initial homotopy path, defined by $\mathbf{\Gamma}_0(\kappa, \boldsymbol{x})$. Since the DCM terminates at limit points, limit points can be detected if the step-size is small enough, and the solution point satisfies $\|\boldsymbol{x}\|_\infty \leq T_h$ where T_h is the threshold defined in Section 3.4.2. When a limit point $\boldsymbol{x}_{L,0}$ is encountered at $\kappa_{L,0}$, another feasible homotopy path defined by $\mathbf{\Gamma}(\kappa, \boldsymbol{x}, \Omega_1)$ is found by searching for a proper Ω_1. Then, the new

starting point $\boldsymbol{x}_{0,1}$ at $\kappa_{L,0}$ triggers a new homotopy path, again tracked by DCM. At $\boldsymbol{x}_{L,1}$, the new homotopy path defined by $\boldsymbol{\Gamma}(\boldsymbol{\kappa}, \boldsymbol{x}, \Omega_2)$ is found and tracked. This process is repeated until the line $\kappa = 1$ is reached.

In general, suppose that the DCM encounters a limit point $\boldsymbol{x}_{L,j-1}$ at $\kappa_{L,j-1}$ while tracking the homotopy path defined by $\boldsymbol{\Gamma}(\kappa, \boldsymbol{x}, \Omega_{j-1})$. The goal is to switch to a new solution curve by finding a new homotopy path defined by $\boldsymbol{\Gamma}(\kappa, \boldsymbol{x}, \Omega_j)$ starting from $\boldsymbol{x}_{0,j}$ at $\kappa_{L,j-1}$. The unknown variables for the j-th homotopy path are Ω_j and $\boldsymbol{x}_{0,j}$; that is, a total of $(m+1) \times n$ unknowns against the n-dimensional consistency condition. The problem is clearly underdetermined, and therefore Ω_j and $\boldsymbol{x}_{0,j}$ are found by solving an optimization problem.

The main feature sought in a candidate homotopy path are feasibility and an easy progression of the DCM. Ideally, one may want to switch to a new feasible horizontal path, which would easily lead to the solution of the objective problem ($\kappa = 1$). In this respect, the projected $\|\boldsymbol{\Gamma}\|_2$ error trend along a candidate homotopy path is considered. In Fig. 5, the projected error is discerned into a near-side error, $\boldsymbol{\Gamma}(\kappa_{L,j-1} + \Delta\kappa, \boldsymbol{x}, \Omega_j)$, and a far-side error $\boldsymbol{\Gamma}(\min(\kappa_{L,j-1} + i\zeta\Delta\kappa, 1), \boldsymbol{x}, \Omega_j)$. The former is minimized to ease restart of the DCM, while the latter is weighted to select a mild path. The problem is therefore to

$$\min_{\Omega_j, \boldsymbol{x}_{0,j}} J \quad \text{s.t.} \quad \boldsymbol{c}_{\text{eq}} = \boldsymbol{0} \tag{3.16}$$

where

$$J \coloneqq \|\boldsymbol{\Gamma}\left(\min(\kappa_{L,j-1} + \Delta\kappa, 1), \boldsymbol{x}_{0,j}, \Omega_j\right)\|_2 + \sum_{i=1}^{N} \gamma^i \|\boldsymbol{\Gamma}\left(\min(\kappa_{L,j-1} + i\zeta\Delta\kappa, 1), \boldsymbol{x}_{0,j}, \Omega_j\right)\|_2 \tag{3.17}$$

and

$$\boldsymbol{c}_{\text{eq}} \coloneqq \begin{cases} \boldsymbol{1}_{n\times 1}, & \text{if } \left|\det\left(\partial\boldsymbol{\Gamma}\left(\kappa_{L,j-1}, \boldsymbol{x}_{0,j}, \Omega_j\right)/\partial\boldsymbol{x}\right)\right| \leq \delta \\ \boldsymbol{\Gamma}\left(\kappa_{L,j-1}, \boldsymbol{x}_{0,j}, \Omega_j\right), & \text{otherwise} \end{cases} \tag{3.18}$$

In (3.17), $\gamma \in [0, 1)$ is a discount factor, ζ is the predicted horizon, and N is the number of predicted points. An artificial violation of the equality constraint in (3.18) is introduced to avoid near-singular paths. Moreover, Ω_{j-1} and $\boldsymbol{x}_{L,j-1}$ are taken as initial guess for the optimization problem in (3.16).

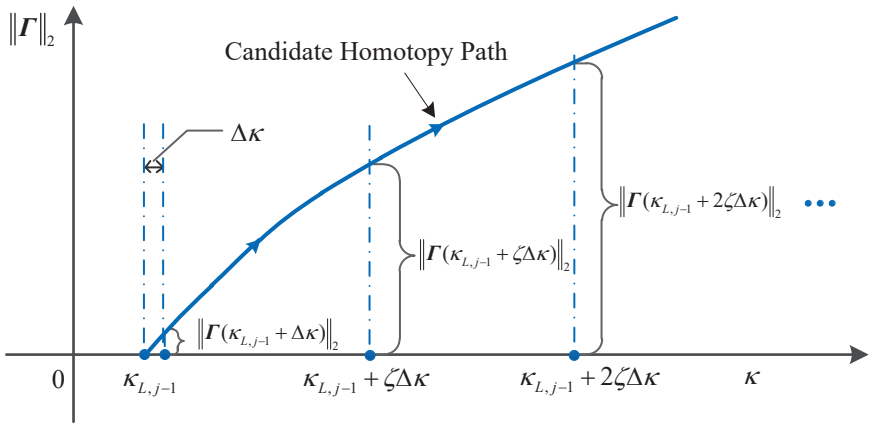

Figure 5: Error trend along a candidate homotopy path.

3.4.2. Indefinite Growth Management

Beside tackling limit points, paths of Type 5 in Fig. 1 are also considered. As shown in Fig. 6, indefinite growth is managed through thresholding. An a-priori threshold T_h on $\|\boldsymbol{x}\|_\infty$ is set. Once the homotopy path crosses the threshold line, the second layer is triggered to switch to an alternative, feasible homotopy path.

In Fig. 6, when the initial homotopy path exceeds T_h, the solution point $\boldsymbol{x}_{\mathrm{I},0}$ at $\kappa_{\mathrm{I},0}$ is detected. This is used as initial guess to solve the optimization problem in (3.16), and a new homotopy path (using Ω_1 and starting from $\boldsymbol{x}_{0,1}$) is tracked. If this new homotopy path exceeds T_h (Failed Case 1) or the solver fails to converge (Failed Case 2), the solution point near but below $T_h/2$ is considered, until a new feasible path is found. In Fig. 6, the new homotopy path defined by $\boldsymbol{\Gamma}(\kappa, \boldsymbol{x}, \Omega_3)$ starting from $\boldsymbol{x}_{0,3}$ at $\kappa_{\mathrm{I},2}$ is found by using $T_h/4$.

The algorithmic rationale of the two-layer, TFC-based homotopy method is summarized in Algorithm 1, where $\Delta\kappa_{\min}$ is the step-size threshold to detect the limit point, and N_s is the total times of path switching.

4. Numerical Experiments

In this section, three numerical experiments are performed using the TFC-based DCM method. To ease assessment of the developed algorithm, the outcome of each problem is compared to the solution obtained using PAM. The zero-finding and optimization problems are solved using Matlab's `fzero`

Algorithm 1 Two-layer TFC-based DCM Algorithm

Require: $\Delta\kappa$, $\Delta\kappa_{\min}$, $\boldsymbol{h}(\kappa, \boldsymbol{x})$, $\boldsymbol{G}(\boldsymbol{x})$, and T_h.
Ensure: Solution to $\boldsymbol{F}(\boldsymbol{x}) = \boldsymbol{0}$.

Set $\kappa = 0$, $\kappa_{\text{old}} = 0$, $j = 0$, $\Delta\kappa_{\text{iter}} = \Delta\kappa$, and $\Omega_0 = 0_{n\times n}$, $N_s = 0$.
Solve the auxiliary problem $\boldsymbol{G}(\boldsymbol{x}) = \boldsymbol{0}$.
while $\kappa < 1$ **do**
  $\kappa \leftarrow \kappa + \Delta\kappa_{\text{iter}}$.
  Solve the zero-finding problem $\boldsymbol{\Gamma}(\kappa, \boldsymbol{x}, \Omega_j) = \boldsymbol{0}$.
  if Converged but the solution satisfies $\|\boldsymbol{x}\|_\infty > T_h$ **then**
    Solve the optimization problem (3.16).
    Switch to the new homotopy path $\boldsymbol{\Gamma}(\kappa, \boldsymbol{x}, \Omega_{j+1})$, $j \leftarrow j + 1$.
    $\Delta\kappa_{\text{iter}} \leftarrow \min(1 - \kappa, \Delta\kappa)$, $\kappa_{\text{old}} \leftarrow \kappa$, $N_s \leftarrow N_s + 1$.
  else
    if Converged **then**
      $\Delta\kappa_{\text{iter}} \leftarrow \min(1 - \kappa, \Delta\kappa)$. $\kappa_{\text{old}} \leftarrow \kappa$.
    else
      if $\Delta\kappa_{\text{iter}} \leq \Delta\kappa_{\min}$ and the solution satisfies $\|\boldsymbol{x}\|_\infty \leq T_h$ **then**
        Solve the optimization problem (3.16).
        Switch to the new homotopy path $\boldsymbol{\Gamma}(\kappa, \boldsymbol{x}, \Omega_{j+1})$, $j \leftarrow j + 1$.
        $\Delta\kappa_{\text{iter}} \leftarrow \min(1 - \kappa, \Delta\kappa)$, $\kappa_{\text{old}} \leftarrow \kappa$, $N_s \leftarrow N_s + 1$.
      else
        $\Delta\kappa_{\text{iter}} \leftarrow \Delta\kappa_{\text{iter}}/2$. $\kappa \leftarrow \kappa_{\text{old}}$.
      end if
    end if
  end if
end while

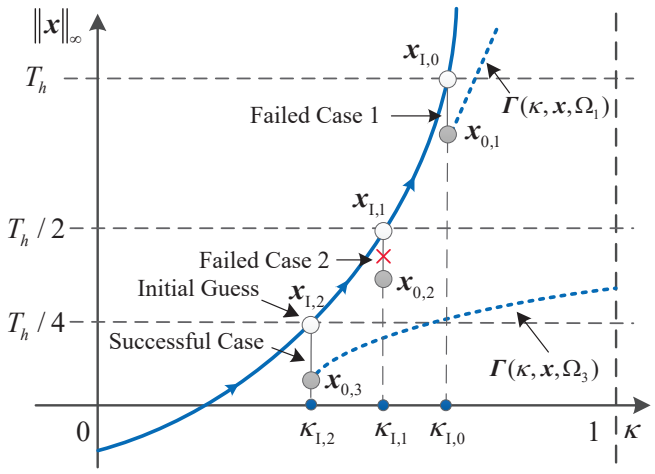

Figure 6: Graphical layout of the indefinite growth management.

and `fmincon` implementing interior-point method, respectively. In both algorithms, the function residual (`TolFun`) and solution tolerance (`TolX`) are both set to 10^{-12}. All test cases have been performed using Matlab R2019a with Intel Core i7-9750H CPU @2.60 GHz, Windows 10 operating system. The parameters of the optimization problem in (3.17)–(3.18) are $\gamma = 0.5$, $\zeta = 15$, $N = 3$, $\delta = 1 \times 10^{-4}$ and $\Delta\kappa_{\min} = 1 \times 10^{-8}$.

4.1. Algebraic Zero-Finding Problem

The zero of the following two-dimensional function is sought [35]

$$\boldsymbol{F}(x_1, x_2) = \begin{bmatrix} a(x_1 + x_2) \\ a(x_1 + x_2) + (x_1 - x_2)\left((x_1 - b)^2 + x_2^2 - c\right) \end{bmatrix} \tag{4.1}$$

where $a = 4, b = 2, c = 1$. The state-dependent basis function $\boldsymbol{h}(\kappa, \boldsymbol{x})$ is

$$\boldsymbol{h}(\kappa, \boldsymbol{x}) = \begin{bmatrix} \mathrm{e}^{x_1}\kappa^2 \\ \mathrm{e}^{x_2}\kappa^2 \end{bmatrix}$$

and $\Delta\kappa = 0.001$.

In [35, 36], it is stated that if the initial condition is located inside the circle $(x_1 - 2)^2 + x_2^2 = 1$, the Newton homotopy function implementing PAM will fail to find the solution. This property is independently confirmed by our numerical experiment. In Fig. 7, Newton homotopy function is used. Both PAM and TFC-based DCM for various initial conditions $\boldsymbol{x}_0$ (the solution to

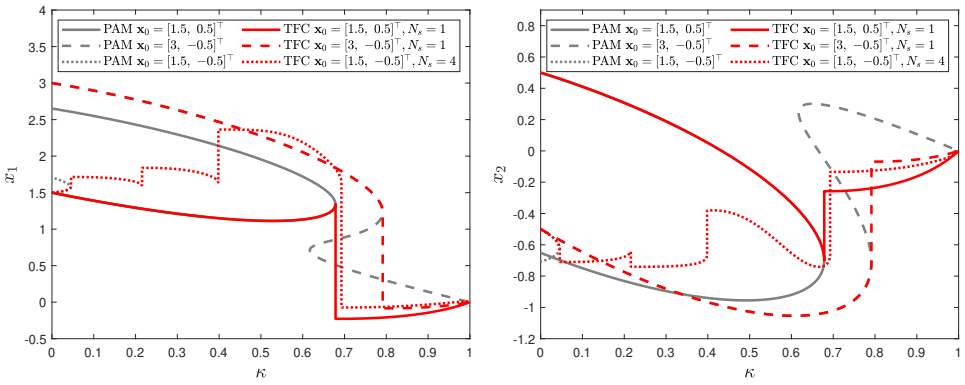

(a) (b)

Figure 7: Homotopy paths generated by the Newton homotopy method using PAM and the TFC-based DCM while attempting to find the zero of the function in (4.1).

$\boldsymbol{G}(\boldsymbol{x}) = \mathbf{0}$) are executed. For cases $\boldsymbol{x}_0 = [1.5, 0.5]^\top$ and $\boldsymbol{x}_0 = [1.5, -0.5]^\top$ inside the disc, PAM effectively passes a singular point but the paths return back to $\kappa = 0$, while the presented method reaches the solution by switching the path $N_s = 1$ and $N_s = 4$ times, respectively. For the case $\boldsymbol{x}_0 = [3, -0.5]^\top$, PAM passes two singular points before reaching the solution, while the presented method switches to another feasible homotopy path that eventually converges to the solution of the objective problem.

When the TFC-based DCM method is used for the case $\boldsymbol{x}_0 = [1.5, 0.5]^\top$, the limit point $\boldsymbol{x}_{L,0} = [1.3406, -0.6978]^\top$ is detected at $\kappa_{L,0} = 0.6786$. Here, the second-layer of the algorithm is triggered, and a new homotopy path is followed, starting from $\boldsymbol{x}_{0,1} = [-0.2269, -0.2570]^\top$ with

$$\Omega_1 = \begin{bmatrix} -15.4518 & -10.7949 \\ -6.7812 & -18.0602 \end{bmatrix}$$

The new homotopy path leads smoothly to $\kappa = 1$ where $\boldsymbol{x}^* = [0, 0]^\top$.

When fixed-point homotopy method is employed, numerical experiments show that it performs worse than Newton homotopy. In Fig. 8, fixed-point homotopy function is used. Both PAM and TFC-based DCM for the same $\boldsymbol{x}_0$ in Fig. 7 are simulated. For all cases, PAM fails and the x_2 paths go to infinity, while the paths generated by the presented method successfully reach the solution after few path switching. Thus, there is evidence that the

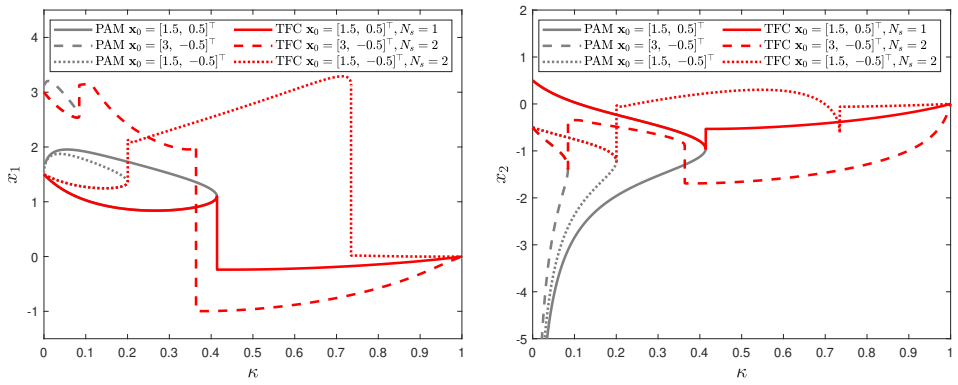

(a) (b)

Figure 8: Homotopy paths generated by the fixed-point homotopy method using PAM and the TFC-based DCM while attempting to find the zero of the function in (4.1).

presented method is robust to different user-defined homotopy functions for the current problem.

From (3.17), it is noticed that the step-size $\Delta\kappa$ affects the selection of the new path. In Fig. 9, the paths generated by the TFC-based DCM method with user-defined fixed-point homotopy function and $\boldsymbol{x}_0 = [2.5, 0.5]^\top$ for various $\Delta\kappa$ are illustrated. It can be seen that when $\Delta\kappa = 0.03$ is used, one more path switching arises compared to other values of $\Delta\kappa$. Thus, smaller values of $\Delta\kappa$ are preferred that favour smooth paths. As a general rule, $\Delta\kappa$ has to be smaller when the problem complexity increases.

Moreover, the effect of number of predicted points N in (3.17) on the new path selection is studied in Fig. 10. It can be seen that the new paths for $N = 8$ and $N = 20$ are very close, implying that the effect of N decreases as N increases if $\boldsymbol{\Gamma}(\kappa, \boldsymbol{x}, \Omega)$ is not abruptly changed when κ varies. Small N are preferred since larger N involve increased computational costs.

4.2. Nonlinear Optimal Control Problem

Solving a nonlinear optimal control problem means find the zero of a shooting function, which solves the associated two-point boundary value problem [37]. Consider the dynamical system

$$\begin{aligned} \dot{x}_1 &= x_1 + x_2 + u_1 \\ \dot{x}_2 &= \tan x_1^2 + u_2 \end{aligned} \tag{4.2}$$

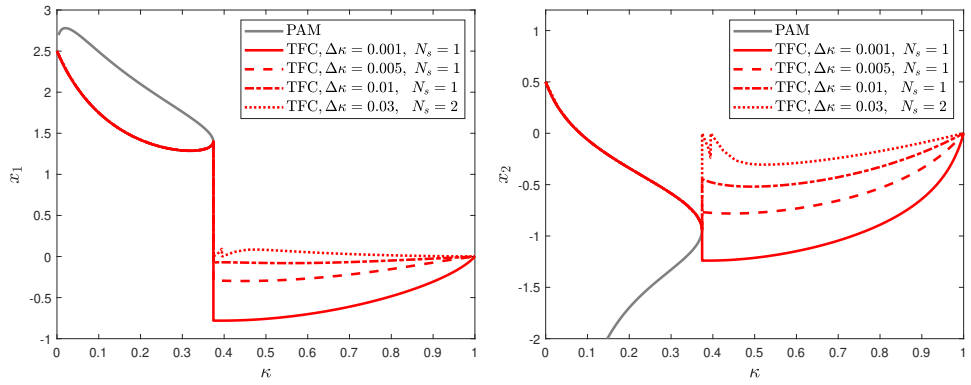

(a) (b)

Figure 9: Homotopy paths generated by the TFC-based DCM method with user-defined fixed-point homotopy function and $\boldsymbol{x}_0 = [2.5, 0.5]^\top$ for different $\Delta\kappa$.

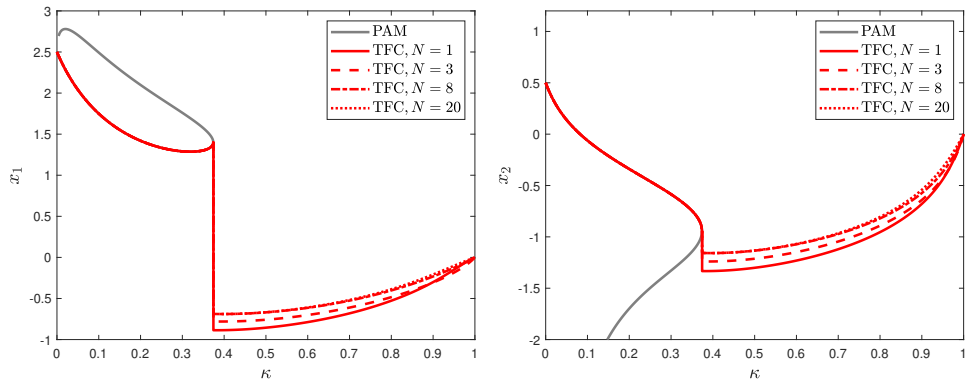

(a) (b)

Figure 10: Homotopy paths generated by the TFC-based DCM method with user-defined fixed-point homotopy function and $\boldsymbol{x}_0 = [2.5, 0.5]^\top$ for different N.

along with the performance index

$$J = \frac{1}{2}\int_0^{t_f} \left(u_1^2 + u_2^2\right) \mathrm{d}t$$

where the terminal time is $t_f = 1$, and the boundary conditions are set to $\boldsymbol{x}_0 = [-1, -1]^\top$ and $\boldsymbol{x}_f = [0, 0]^\top$. An homotopy from linear to nonlinear dynamics is constructed by embedding κ into (4.2), i.e.,

$$\begin{aligned} \dot{x}_1 &= x_1 + x_2 + u_1 \\ \dot{x}_2 &= \kappa \tan x_1^2 + u_2 \end{aligned}$$

Based on the optimal control theory [37], the Euler–Lagrange equations are

$$\begin{aligned} \dot{x}_1 &= x_1 + x_2 - \lambda_1 \\ \dot{x}_2 &= \kappa \tan x_1^2 - \lambda_2 \\ \dot{\lambda}_1 &= -\lambda_1 - 2\kappa x_1 \lambda_2 / \cos^2 x_1^2 \\ \dot{\lambda}_2 &= -\lambda_1 \end{aligned} \tag{4.3}$$

For a given κ, the flow $\boldsymbol{x}(t, \boldsymbol{x}_0, \boldsymbol{\lambda}_0)$ can be obtained by integrating (4.3) with initial conditions $\boldsymbol{x}_0$ and $\boldsymbol{\lambda}_0$, where $\boldsymbol{\lambda}_0 = [\lambda_1(t_0), \lambda_2(t_0)]^\top$ is the initial costate vector. The zero-finding problem is to find $\boldsymbol{\lambda}_0$ such that $\boldsymbol{F}(\boldsymbol{\lambda}_0) = \boldsymbol{0}$, where

$$\boldsymbol{F}(\boldsymbol{\lambda}_0) = \boldsymbol{x}(t_f, \boldsymbol{x}_0, \boldsymbol{\lambda}_0) - \boldsymbol{x}_f$$

When $\kappa = 0$, the system is linear, and the corresponding initial costate is $\boldsymbol{\lambda}_0 = [-2.9411, -2.0820]^\top$. In this example, the state-dependent function $\boldsymbol{h}(\kappa, \boldsymbol{\lambda})$ is selected as

$$\boldsymbol{h}(\kappa, \boldsymbol{\lambda}) = \begin{bmatrix} \mathrm{e}^{\lambda_1}\kappa^2 \\ \mathrm{e}^{\lambda_2}\kappa^2 \end{bmatrix}$$

and $\Delta\kappa = 0.001$.

The simulation results are shown in Fig. 11, where the comparison of the homotopy paths for PAM (grey dashed line) and TFC-based DCM (red solid line) is shown in Fig. 11a, whereas the optimal trajectory is shown in Fig. 11b. Notice that in Fig. 11a the solution curve tracked by PAM successfully passes a limit point but returns back to $\kappa \simeq 0$. PAM fails to reach the solution to the objective problem at $\kappa = 1$.

When the TFC-based DCM method is used, the limit point $\boldsymbol{\lambda}_{L,0} = [-1.2251, -1.5879]^\top$ is detected at $\kappa_{L,0} = 0.5376$. The second layer switches

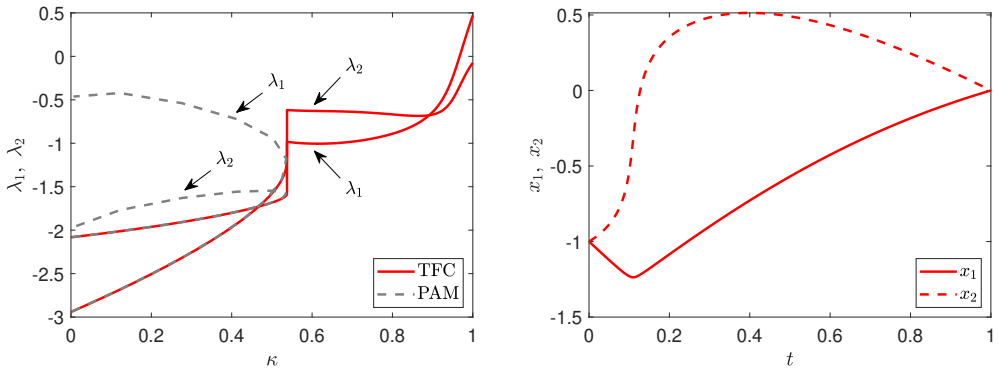

(a) (b)

Figure 11: Simulation results for the nonlinear optimal control problem. (a): Comparison of homotopy paths tracked by PAM and TFC-based DCM method; (b): Optimal trajectories $x_1(t)$ and $x_2(t)$.

to a new homotopy path starting from $\boldsymbol{\lambda}_{0,1} = [-0.9834, -0.6184]^\top$ with

$$\Omega_1 = \begin{bmatrix} -5.7765 & -4.1086 \\ -7.6160 & 5.7975 \end{bmatrix}$$

The new homotopy path leads smoothly to the solution of the objective problem, where $\boldsymbol{\lambda}^*(t_0) = [0.4728, -0.0739]^\top$.

4.3. Elastic Rod Problem

While in Sections 4.1 and 4.2 the issue was overcoming a singular point (Type 1, 3, and 4 in Fig. 1), in this example the path goes off to infinity without encountering any limit point (Type 5 in Fig. 1). The cantilever beam problem, which is to find the position (a, b) of the tip of the rod given the force $Q \neq 0$ and $P = 0$, has a closed-form solution in terms of elliptic integrals. The inverse problem, where the tip's position (a, b) and orientation c are specified, while the forces (Q, P) and torque (M) are to be determined, has no similar closed-form solution. It is a nonlinear problem that is difficult to solve [38]. The inverse problem is solved in this section. The dynamic equations

$$\begin{aligned} \dot{x} &= \cos\theta \\ \dot{y} &= \sin\theta \\ \dot{\theta} &= Qx - Py + M \end{aligned}$$

are supported by the boundary conditions

$$x(0) = y(0) = \theta(0) = 0, \quad x(1) = a, \quad y(1) = b, \quad \theta(1) = c$$

The unknown variables are denoted as $\boldsymbol{v} = [Q, P, M]^\top$, and the corresponding flow is denoted as $x(t, \boldsymbol{v}), y(t, \boldsymbol{v}), \theta(t, \boldsymbol{v})$. The problem is to find $\boldsymbol{v}^*$ such that

$$\boldsymbol{F}(\boldsymbol{v}^*) = \begin{bmatrix} x(t_f, \boldsymbol{v}^*) - a \\ y(t_f, \boldsymbol{v}^*) - b \\ \theta(t_f, \boldsymbol{v}^*) - c \end{bmatrix} = \boldsymbol{0} \tag{4.4}$$

A fixed-point homotopy function is defined as

$$\boldsymbol{\Gamma}_0(\kappa, \boldsymbol{v}) = (1 - \kappa)\boldsymbol{F}(\boldsymbol{v}) + \kappa \boldsymbol{G}(\boldsymbol{v}) \quad \text{with} \quad \boldsymbol{G}(\boldsymbol{v}) = (\boldsymbol{v} - \boldsymbol{v}_0)$$

where $\boldsymbol{v}_0$ is the initial guess solution. The parameters are set to $a = 0$, $b = 2\pi$, $c = \pi$, and $\boldsymbol{v}_0 = [0, 0, 1.85]^\top$. In this case, the solution to the objective problem in (4.4) is known to be $\boldsymbol{v}^* = [0, 0, \pi]^\top$ [39]. The Jacobian matrix of (4.4) w.r.t $\boldsymbol{v}$ has been computed using finite differences, and the limit threshold T_h is set to 100. The selected state-dependent basis function $\boldsymbol{h}(\kappa, \boldsymbol{v})$ is

$$\boldsymbol{h}(\kappa, \boldsymbol{v}) = \begin{bmatrix} \mathrm{e}^Q \kappa^2 \\ \mathrm{e}^P \kappa^2 \\ \mathrm{e}^M \kappa^2 \end{bmatrix}$$

and $\Delta\kappa = 0.001$.

The simulation results are shown in Fig. 12, where the homotopy paths generated by PAM (grey lines) and TFC-based DCM (red lines) are shown (Fig. 12b shows an enlarged view of Fig. 12a when $\kappa \to 1$). PAM is not able to reach $\boldsymbol{v}^*$ because the homotopy path grows indefinitely when $\kappa \to 1$.

Using TFC-based DCM, the failure of the initial homotopy path is detected when $\|\boldsymbol{v}\|_\infty$ exceeds T_h. The point $\boldsymbol{v}_{\mathrm{I},0} = [-99.2011, -50.7766, 11.0163]^\top$ at $\kappa_{\mathrm{I},0} = 0.9965$ is used as initial guess for problem (3.16). A new start point $\boldsymbol{v}_{0,1} = [-99.1925, -50.7788, 11.0155]^\top$ is found, with

$$\Omega_1 = \begin{bmatrix} 0 & 0 & -2.56 \times 10^{-5} \\ 0 & 0 & -1.60 \times 10^{-5} \\ 0 & 0 & 3.21 \times 10^{-4} \end{bmatrix}$$

which is very close to the initial path. Since this homotopy path excesses T_h again, a second switch is attempted using $T_h/2$. The initial guess $\boldsymbol{v}_{\mathrm{I},1} =$

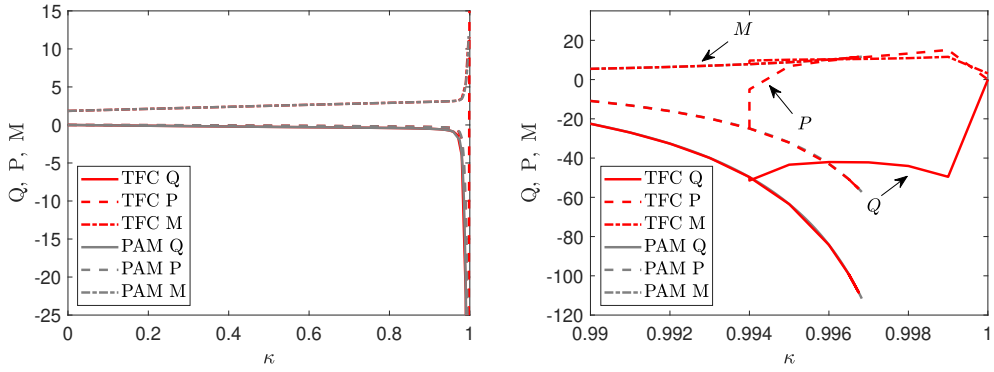

(a) (b)

Figure 12: Simulation results for elastic red problem. (a): Comparison of homotopy paths tracked by PAM (grey dashed lines) and TFC-based DCM (red solid lines); (b): Zoom-in comparison of homotopy paths when $\kappa \to 1$.

$[-49.6995, -24.9227, 7.8530]^\top$ at $\kappa_{\mathrm{I},1} = 0.9940$ is detected, and problem (3.16) is solved gain. The new homotopy path with starting point $\boldsymbol{v}_{0,2} = [-51.4515, -4.9992, 9.6862]^\top$ and

$$\Omega_2 = \begin{bmatrix} 0 & 9.03 \times 10^{-6} & -2.60 \times 10^{-3} \\ 0 & -1.60 \times 10^{-6} & 1.73 \times 10^{-3} \\ 0 & 1.27 \times 10^{-5} & 7.44 \times 10^{-4} \end{bmatrix}$$

is found. From this point on, the TFC-based DCM successfully reaches $\boldsymbol{v}^*$.

5. Conclusion

Homotopy is a deformation used in zero-finding problems. The idea is to connect an initial easy-to-solve problem to the final, objective problem through the solution of a number of intermediate, auxiliary problems that define the homotopy path. Traditional techniques based on pure DCM or PAM fail to reach the objective problem, e.g., when the homotopy path exhibits singular points or indefinite growth. The fate of these methods is already determined when the homotopy function is formulated and the initial condition is given.

The TFC-based homotopy function presented in this paper implicitly defines infinite homotopy paths. This property can be leveraged whenever

either a singularity is found or the path tends to go off to infinity. In these cases, the algorithm is able to switch to a new homotopy path, which attempts to reach the objective problem. A two-layer TFC-based DCM algorithm has been developed to support our intuition. The effectiveness of this algorithm has been proved by solving sample problems where the traditional continuation methods fail.

Future work will investigate the following aspects to enhance the robustness of TFC-based homotopy method: (1) Current method to search a new path is inefficient for the large-scale problems. Methods with high computational efficiency such as convex programming, least-square methods or Lyapunov methods, etc., are worth to explore. (2) The presented method is a local continuation method, yet it is a valuable direction towards designing probability-one homotopy methods for general applications.

6. Acknowledgment

Y.W. acknowledges the support of the China Scholarship Council (Grant no.201706290024). The authors would like to thank Prof. Daniele Mortari for the fruitful discussions on the Theory of Functional Connections.

References

[1] D. R. Easterling, L. T. Watson, N. Ramakrishnan, Probability-one homotopy methods for constrained clustering, J. Comput. Appl. Math. 343 (2018) 602–618. doi:10.1016/j.cam.2018.04.035.

[2] T. Haberkorn, P. Martinon, J. Gergaud, Low-thrust minimum-fuel orbital transfer: a homotopic approach, J. Guid. Control Dyn. 27 (2004) 1046–1060. doi:10.2514/1.4022.

[3] R. Bulirsch, F. Montrone, H. J. Pesch, Abort landing in the presence of windshear as a minimax optimal control problem, part 2: multiple shooting and homotopy, J. Optim. Theory Appl. 70 (1991) 223–254. doi:10.1007/BF00940625.

[4] A. Hermant, Optimal control of the atmospheric reentry of a space shuttle by an homotopy method, Optim. Control Appl. Methods 32 (2011) 627–646. doi:10.1002/oca.961.

[5] S. Ji, L. T. Watson, L. Carin, Semisupervised learning of hidden markov models via a homotopy method, IEEE Trans. Pattern Anal. 31 (2009) 275–287. doi:10.1109/TPAMI.2008.71.

[6] E. L. Allgower, K. Georg, Introduction to Numerical Continuation Methods, SIAM, Philadelphia, 2003. doi:10.1137/1.9780898719154.

[7] S. K. Rahimian, F. Jalali, J. D. Seader, R. E. White, A new homotopy for seeking all real roots of a nonlinear equation, Comput. Chem. Eng. 35 (2011) 403–411. doi:10.1016/j.compchemeng.2010.04.007.

[8] Y. Dai, S. Kim, M. Kojima, Computing all nonsingular solutions of cyclic-n polynomial using polyhedral homotopy continuation methods, J. Comput. Appl. Math. 152 (2003) 83–97. doi:10.1016/S0377-0427(02)00698-2.

[9] T.-M. Wu, Solving the nonlinear equations by the Newton-homotopy continuation method with adjustable auxiliary homotopy function, Appl. Math. Comput. 173 (2006) 383–388. doi:10.1016/j.amc.2005.04.095.

[10] B. Pan, P. Lu, X. Pan, Y. Ma, Double-homotopy method for solving optimal control problems, J. Guid. Control Dyn. 39 (2016) 1706 – 1720. doi:10.2514/1.G001553.

[11] B. Pan, X. Pan, S. Zhang, A new probability-one homotopy method for solving minimum-time low-thrust orbital transfer problems, Astrophys. Space Sci. 363 (2018) 198. doi:10.1007/s10509-018-3420-0.

[12] T. Ohtsuka, H. Fujii, Stabilized continuation method for solving optimal control problems, J. Guid. Control Dyn. 17 (1994) 950–957. doi:10.2514/3.21295.

[13] G. R. Kotamraju, M. R. Akella, Stabilized continuation methods for boundary value problems, Appl. Math. Comput. 112 (2000) 317–332. doi:10.1016/S0096-3003(99)00061-2.

[14] T. Haberkorn, P. Martinon, J. Gergaud, Low-thrust minimum-fuel orbital transfer: a homotopic approach, J. Guid. Control Dyn. 27 (2004) 1046–1060. doi:10.2514/1.4022.

[15] W. Hao, C. Zheng, An adaptive homotopy method for computing bifurcations of nonlinear parametric systems, J. Sci. Comput. 82 (2020) 53. doi:10.1007/s10915-020-01160-w.

[16] C. Carstensen, J. Gedicke, V. Mehrmann, A. Miedlar, An adaptive homotopy approach for non-selfadjoint eigenvalue problems, Numer. Math. 119 (2011) 557–583. doi:10.1007/s00211-011-0388-x.

[17] D. J. Bates, J. D. Hauenstein, A. J. Sommese, Efficient path tracking methods, Numer. Algorithms 58 (2011) 451–459. doi:10.1007/s11075-011-9463-8.

[18] D. A. Brown, D. W. Zingg, A monolithic homotopy continuation algorithm with application to computational fluid dynamics, J. Comput. Phys. 321 (2016) 55–75. doi:10.1016/j.jcp.2016.05.031.

[19] D. A. Brown, D. W. Zingg, Monolithic homotopy continuation with predictor based on higher derivatives, J. Comput. Appl. Math. 346 (2019) 26–41. doi:10.1016/j.cam.2018.06.036.

[20] K. Yamamura, Simple algorithms for tracing solution curves, IEEE Trans. Circuits-I 40 (1993) 537–541. doi:10.1109/81.242328.

[21] R. Kalaba, L. Tesfatsion, Solving nonlinear equations by adaptive homotopy continuation, Appl. Math. Comput. 41 (1991) 99–115. doi:10.1016/0096-3003(91)90064-T.

[22] D. M. Wolf, S. R. Sanders, Multiparameter homotopy methods for finding DC operating points of nonlinear circuits, IEEE Trans. Circuits-I 43 (1996) 824–838. doi:10.1109/81.538989.

[23] T. L. Wayburn, J. D. Seader, Homotopy continuation methods for computer-aided process design, Comput. Chem. Eng. 11 (1987) 7–25. doi:10.1016/0098-1354(87)80002-9.

[24] J. Nocedal, S. Wright, Numerical Optimization, second ed., Springer, New York, 2006. doi:10.1007/978-0-387-40065-5, p. 296–302.

[25] S. Liao, Homotopy Analysis Method in Nonlinear Differential Equations, Springer and Higher Education Press, Berlin and Beijing, 2012. doi:10.1007/978-3-642-25132-0.

[26] S. Liao, On the homotopy analysis method for nonlinear problems, Appl. Math. Comput. 147 (2004) 499–513. doi:10.1016/S0096-3003(02)00790-7.

[27] S. Liao, Notes on the homotopy analysis method: some definitions and theorems, Commun. Nonlinear Sci. 14 (2009) 983–997. doi:10.1016/j.cnsns.2008.04.013.

[28] D. Mortari, The theory of connections: connecting points, Mathematics 5 (2017) 57. doi:10.3390/math5040057.

[29] C. Leake, H. Johnston, D. Mortari, The multivariate theory of functional connections: theory, proofs, and application in partial differential equations, Mathematics 8 (2020) 1303. doi:10.3390/math8081303.

[30] D. Mortari, C. Leake, The multivariate theory of connections, Mathematics 7 (2019) 296. doi:10.3390/math7030296.

[31] D. Mortari, H. Johnston, L. Smith, High accuracy least-squares solutions of nonlinear differential equations, J. Comput. Appl. Math. 352 (2019) 293–307. doi:10.1016/j.cam.2018.12.007.

[32] A. Bhaya, F. A. Pazos, Homotopy methods for zero finding from a learning/control Liapunov function viewpoint, 2013 International Conference on Control, Decision and Information Technologies (CoDIT) (2013) 881–886. doi:10.1109/CoDIT.2013.6689659.

[33] L. T. Watson, Probability-one homotopies in computational science, J. Comput. Appl. Math. 140 (2002) 785–807. doi:10.1016/S0377-0427(01)00473-3.

[34] S. N. Chow, J. Mallet-Paret, J. A. Yorke, Finding zeroes of maps: homotopy methods that are constructive with probability one, Math. Comput. 32 (1978) 887–899. doi:10.1090/S0025-5718-1978-0492046-9.

[35] F. H. Branin, Widely convergent method for finding multiple solutions of simultaneous nonlinear equations, IBM J. Res. Dev. 16 (1972) 504–522. doi:10.1147/rd.165.0504.

[36] P. J. Zufiria, R. S. Guttalu, On the role of singularities in Branin's method from dynamic and continuation perspectives, Appl. Math. Comput. 130 (2002) 593–618. doi:10.1016/S0096-3003(01)00120-5.

[37] A. E. Bryson, Y.-C. Ho, Applied Optimal Control: Optimization, Estimation and Control, Taylor and Francis, New York, 1975. doi:10.1201/9781315137667.

[38] L. T. Watson, Globally convergent homotopy methods: a tutorial, Appl. Math. Comput. 31 (1989) 369–396. doi:10.1016/0096-3003(89)90129-X.

[39] L. T. Watson, C. Y. Wang, A homotopy method applied to elastica problems, Int. J. Solids Struct. 17 (1981) 29–37. doi:10.1016/0020-7683(81)90044-5.